RESEARCH ARTICLE | JUNE 04 2024

Genetic programing control of self-excited thermoacoustic oscillations

Bo Yin ; Zhijian Yang ; Yu Guan ; Stephane Redonnet ; Vikrant Gupta ; Larry K. B. Li

Physics of Fluids 36, 064102 (2024)
https://doi.org/10.1063/5.0211639

Physics of Fluids ARTICLE pubs.aip.org/aip/pof

Genetic programing control of self-excited thermoacoustic oscillations

Cite as: Phys. Fluids **36**, 064102 (2024); doi: 10.1063/5.0211639
Submitted: 1 April 2024 · Accepted: 16 May 2024 ·
Published Online: 4 June 2024

Bo Yin,[1] Zhijian Yang,[1] Yu Guan,[2] Stephane Redonnet,[1] Vikrant Gupta,[3,4] and Larry K. B. Li[1,5,a)]

AFFILIATIONS

[1]Department of Mechanical and Aerospace Engineering, The Hong Kong University of Science and Technology, New Territories, Hong Kong
[2]Department of Aeronautical and Aviation Engineering, The Hong Kong Polytechnic University, Kowloon, Hong Kong
[3]Guangdong Provincial Key Laboratory of Turbulence Research and Applications, Department of Mechanics and Aerospace Engineering, Southern University of Science and Technology, Shenzhen, China
[4]Guangdong-Hong Kong-Macao Joint Laboratory for Data-Driven Fluid Mechanics and Engineering Applications, Southern University of Science and Technology, Shenzhen, China
[5]Guangdong-Hong Kong-Macao Joint Laboratory for Data-Driven Fluid Mechanics and Engineering Applications, The Hong Kong University of Science and Technology, New Territories, Hong Kong

[a)]**Author to whom correspondence should be addressed:** larryli@ust.hk

ABSTRACT

In this experimental study, we use a data-driven machine learning framework based on genetic programing (GP) to discover model-free control laws (individuals) for suppressing self-excited thermoacoustic oscillations in a prototypical laminar combustor. This GP framework relies on an evolutionary algorithm to make decisions based on natural selection. Starting from an initial generation of individuals, we rank their performance based on a cost function that accounts for the trade-off between the state cost (thermoacoustic amplitude) and the input cost (actuator power). We then breed subsequent generations of individuals via a tournament in which the direct forwarding of elite individuals occurs alongside genetic operations such as mutation, replication, and crossover. We implement this GP control framework in both closed-loop and open-loop forms, followed by benchmarking against conventional open-loop control based on time-periodic forcing. We find that while all three control strategies can achieve similarly large reductions in thermoacoustic amplitude, GP closed-loop control consumes the least actuator power, making it the most efficient. It achieves this efficiency by learning an actuation mechanism that exploits the strong heat-release-rate amplification of the open flame at its preferred mode, even though the GP algorithm has never seen the open flame itself. This study demonstrates the feasibility of using GP to discover new and more efficient model-free individuals for suppressing self-excited thermoacoustic oscillations, providing a promising approach to data-driven feedback control of combustion devices.

I. INTRODUCTION

In gas turbines and rocket engines, the coupled interactions between unsteady heat release and sound can generate large-amplitude self-excited flow oscillations, known as thermoacoustic instability.[1,2] If left uncontrolled, such oscillations can damage the system hardware and exacerbate pollutant emissions, impairing reliability, efficiency, and operability.[3]

Thermoacoustic instability can be controlled with passive or active methods.[4] With either method, the goal is to weaken the thermoacoustic driving mechanisms (e.g., mixture-strength coupling, flow instabilities, entropy waves) and/or strengthen the damping mechanisms.[3,5–7] Passive control is usually preferred as it does not require an external energy input, but its implementation requires a detailed understanding of the thermoacoustic feedback processes.[1,8] This understanding is not always attainable owing to the nonlinearity and sensitivity of the multi-scale interactions among combustion, hydrodynamics, and acoustics.[9–12] Active control in the form of open-loop time-periodic forcing, referred to hereafter as open-loop control (OLC), can be effective even without a detailed understanding of the system,[13–16] but it tends to adapt poorly to changes in operating

conditions.[17,18] By contrast, closed-loop control can adapt more readily, but most feedback algorithms are designed around a low-order model of the thermoacoustic system,[19–21] which is not always available or reliable. It is thus helpful to explore alternative approaches to closed-loop control that do not require a system model.

In this experimental study, we use a data-driven framework known as machine learning (ML) control,[22] or more precisely *genetic programing* (GP) control,[23] to discover model-free control laws for suppressing self-excited thermoacoustic oscillations in combustion systems. This framework relies on an evolutionary algorithm to make decisions based on natural selection: a group of *individuals* (i.e., candidate control laws), which are collectively known as a *generation*, compete at a control task defined by a cost function.[22] The performance of each individual is evaluated, and specific rules are set to spread the genes of successful individuals to the next generation. In this way, optimal solutions can be found in a search space containing many dimensions and extrema.[22]

GP improves on a common type of evolutionary algorithm known as genetic algorithms (GAs). While GAs are limited to optimizing the parameters of a *predefined* control law (i.e., for controller tuning), GP enables the optimization of both the control-law structure and its parameters, expanding the search space for model-free individuals.[23] GP also improves on artificial neural networks by outputting the control law as a functional expression, which can be analyzed to gain insight into the flow physics. GP control has been benchmarked on low-order dynamical systems,[22] revealing that (i) it can outperform linear control in weakly nonlinear systems and (ii) it can identify the strongly nonlinear actuation mechanisms in systems with uncontrollable linear dynamics.

In fluid mechanics, GP has been successfully applied to various control problems. In seminal experiments, Gautier *et al.*[24] used GP closed-loop control (GCC) to shrink the recirculation zone behind a backward-facing step, with actuation provided by a slotted jet and sensing provided by particle image velocimetry. They found that after just 12 generations, GCC can outperform the best OLC strategy. This was achieved by learning a novel actuation mechanism: rather than exciting the Kelvin–Helmholtz mode of the shear layers, the optimal GCC law excites the low-frequency flapping mode of the recirculation bubble.[24] Shortly after, Debien *et al.*[25] used a similar GCC strategy to limit the separation of a turbulent boundary layer, with actuation provided by active vortex generators and sensing provided by hot-film and pressure transducers. Again, GCC was found to outperform the best OLC strategy, but this time, the actuation mechanism worked by enhancing the growth rate of the shear layer, rather than by locking in the shedding mode via forced synchronization.[25] Meanwhile, Parezanović *et al.*[26] showed that GCC can outperform OLC in inducing synchronization in a turbulent shear layer. In recent years, various forms of GP control have been demonstrated on many other flow problems, such as reducing the aerodynamic drag of a car,[27] stabilizing the wake of a triple-cylinder cluster (a fluidic pinball),[28] and enhancing mixing in jet flows.[29]

In combustion, Liu *et al.*[30] explored the use of GP to suppress self-excited thermoacoustic oscillations. They showed that GP open-loop control (GOC), as implemented via linear GP, can outperform conventional OLC in reducing the thermoacoustic amplitude and NO_x emissions of a lean premixed flame in a tube combustor. In the present study, we extend the work of Liu *et al.*[30] in several ways. First, rather than applying only GOC and time-periodic OLC, we apply GCC as well, using a single sensor (pressure transducer) and a single actuator (loudspeaker). Crucially, unlike in previous work,[30] our actuator signal is not limited to square waveforms but can take on arbitrary waveforms. Second, rather than including just the state cost (thermoacoustic amplitude) in the cost function, we include the input cost as well, accounting explicitly for the actuator power required to produce a given reduction in the thermoacoustic amplitude. Third, while Liu *et al.*[30] used averaged flame images and Rayleigh index maps to attribute the efficacy of GOC to an impairment in convective flame motion, we attempt to explain the actuation mechanism in terms of the receptivity of the open flame response. All three of these extensions are fundamental. In the first extension, we introduce feedback in the real-time control loop, switching from GOC with square actuator waveforms to GCC with arbitrary actuator waveforms. In the second extension, our inclusion of the input cost (actuator power) in the cost function enables the preferred mode of the open flame to be identified as the key actuation mechanism, yielding the third extension.

The key aims of this study are (i) to experimentally demonstrate that self-excited thermoacoustic oscillations can be efficiently suppressed via a data-driven ML framework based on GCC; (ii) to benchmark the model-free individuals from GCC against those from GOC and OLC; and (iii) to uncover the actuation mechanisms by which GP can suppress self-excited thermoacoustic oscillations. Although practical combustion devices are almost always turbulent, we focus here on a laminar system so as to validate the GP control framework and establish baseline individuals in a relatively quiet environment with only limited degrees of freedom, free from turbulence-induced noise and its associated effects.[18,31–33] Validating GP control in this way should open up further opportunities for its application to turbulent combustors.

II. EXPERIMENTAL SETUP

The experimental setup, shown in Fig. 1, is identical to that used in our previous studies on the forced synchronization of self-excited thermoacoustic oscillations.[16,34–36] Its design is based on a flame-driven Rijke tube:[37] a central burner tube (inner diameter, ID 16.8 mm; length 800 mm; stainless steel) capped with an extension tip (exit ID of $D = 12$ mm; length 30 mm; copper) is used to generate a laminar premixed flame (LPG–air mixture) in a tube combustor with open boundaries at both ends (ID 44 mm; length 860 mm; quartz). The premixed flame is located at $z/L = 0.58$, where z is the distance from the exit of the extension tip to the bottom of the combustor whose total length is L. The volumetric flow rates of air and LPG are 10.5 and 0.22 standard liters per minute (SLPM), respectively. This yields a bulk reactant velocity of $\bar{u} = 1.6$ m/s ($\pm 0.6\%$), an equivalence ratio of 0.62 ($\pm 3.2\%$), a thermal flame power of 430 W ($\pm 4.6\%$), and a Reynolds number of $Re \equiv \rho \bar{u} D/\mu = 1300$ ($\pm 1.2\%$), where ρ and μ are the density and the dynamic viscosity of the reactant mixture, respectively. This operating condition is identical to that of our previous study,[16] providing an established baseline.

For actuation, a loudspeaker (FaitalPRO 6FE100) driven by a power amplifier is used to generate acoustic perturbations to the flame. For sensing, a probe microphone (GRAS 40SA; sensitivity 3 mV/Pa; $\pm 2.5 \times 10^{-5}$ Pa) is used to measure the thermoacoustic amplitude in terms of the pressure fluctuations in the combustor, p'. In our GP control experiments, the microphone is mounted near the middle of the combustor ($z/L = 0.45$) as this is near the pressure anti-node (see Sec.

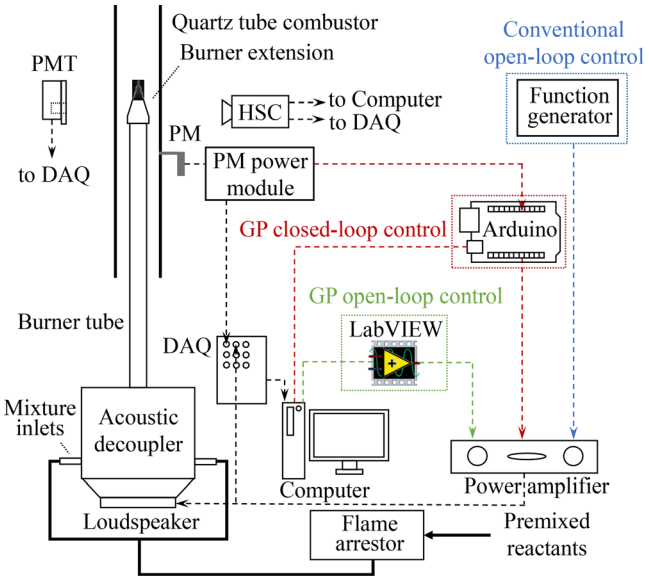

FIG. 1. Schematic of the experimental setup consisting of a flame-driven Rijke tube acted on by three different control strategies: GCC, GOC, and OLC. The measurement diagnostics include a probe microphone (PM), a photomultiplier tube (PMT), and a high-speed camera (HSC, not used). The PM output (acoustic pressure, p') is the main sensor signal.

IV A), boosting the signal-to-noise ratio. The heat-release-rate (HRR) fluctuations of the flame, q', are measured via its CH^* chemiluminescence emission using a photomultiplier tube (Thorlabs PMM01) equipped with a bandpass optical filter (430 nm). For post-processing, the microphone, photomultiplier, and loudspeaker signals are recorded simultaneously at 10 kHz using a data acquisition device (DAQ: NI USB-6356). The computing hardware used for GP control will be discussed in Sec. III.

III. GP CONTROL FRAMEWORK

The GCC framework consists of two main loops:[22] (i) a slow loop for discovering closed-loop individuals via GP and (ii) a fast loop for the real-time application of the closed-loop individuals discovered in the slow loop. The fast loop is therefore a classic feedback control loop, which is hosted on a 32-bit programable microcontroller (Arduino Due; Fig. 1). This loop takes a sensor signal from the probe microphone, processes it via a GP individual, and outputs an actuation signal to the loudspeaker, as per the hardware discussed in Sec. II.

The slow GP loop has three main steps, as shown in Fig. 2: (i) initializing a generation, (ii) evaluating a generation, and (iii) breeding further generations. In this study, we express the GCC laws, which are the individuals populating a generation,[23] as syntax trees (bottom left of Fig. 2). The leaves (squares) of a syntax tree denote constants or inputs, while the nodes (circles) denote basic functions and operators (Table I). The actuation signal fed into the power amplifier (control output) is expressed mathematically as $b_i^j = K_i^j(x)$, where K_i^j is the ith individual of the jth generation. The input signal is defined as $x \equiv p'/\langle|p'_*|\rangle_T$, which is the instantaneous pressure fluctuation with control (p') normalized by the average fluctuation amplitude without control ($\langle|p'_*|\rangle_T$), where $\langle\cdot\rangle_T$ denotes time averaging over interval $T = 2$ s. We initialize the first generation with $N_s = 100$ individuals to create a relatively large initial search space, enhancing the genetic diversity of the population (Table I). In subsequent generations, we use a smaller value of $N_s = 60$ to reduce the GP training time without sacrificing control performance.

After initializing the first generation of individuals, we evaluate them using the cost function $J = \langle S\rangle_{T_e} + \xi\langle|B'|\rangle_{T_e}$, where $T_e = 2$ s is the evaluation time, $S \equiv |p'|/\langle|p'_*|\rangle_T$, and $|B'|$ is the voltage fluctuation amplitude fed into the loudspeaker, after passing through the power amplifier. Thus, the cost function is the sum of the state cost (thermoacoustic amplitude) and the input cost (actuator power), whose relative weighting is set with the penalization coefficient ξ; a low (high) value of ξ favors (sacrifices) performance over economy. We use $\xi = 1.5$ based on the success of previous GP experiments.[22] We apply each individual for 8 s, using the final $T_e = 2$ s to evaluate J, before deactivating the individual. Then, we allow for a dwell time of 6 s before applying the next individual. Given that the transient response time of the system is around 1 s [Fig. 5(a)], these time intervals are long enough for the controlled system to reach a statistically stationary state and for the uncontrolled system to return to its natural self-excited state.

To breed the next generation, we rank all the individuals in the current generation using a tournament based on J_i^j. The new generation has three components:[22,23] (i) elite individuals, which are top-performing individuals forwarded without modification from the current generation; (ii) individuals bred via genetic operations, such as crossover, mutation, and replication; and (iii) freshly generated individuals to maintain genetic diversity. Here, replication involves randomly selecting branches of individuals and forwarding them to the next generation; mutation involves randomly replacing certain branches; and crossover involves randomly selecting two elite individuals and swapping some of their branches. We set the probability of each genetic operation (P_c for crossover, P_m for mutation, and P_r for replication) by considering a balance between (i) introducing new branches, which enhances genetic diversity, and (ii) exploiting existing successful branches, which aids in convergence.[22] The GP algorithm can accept a range of probability combinations, but typically $P_c > P_m > P_r$. For example, previous studies have used combinations such as $(P_c, P_m, P_r) = (0.7, 0.2, 0.1)$,[24,25,28] $(0.6, 0.3, 0.1)$,[30] and $(0.5, 0.4, 0.1)$.[27,38] A high P_c accelerates convergence, while a high P_m promotes exploration and hence genetic diversity. In our GP experiments, we use the combination $(P_c, P_m, P_r) = (0.5, 0.4, 0.1)$ to balance genetic diversity and convergence. Moreover, the number of function operations is determined by the depth (i.e., the number of levels or layers) of the syntax tree, which is the maximum distance between any leaf and the root.[22] We set the depth to be between 3 and 8, balancing complexity and computational cost. As is typical for GP control,[22,24] we prescreen each individual to ensure that its output contains only real numbers with magnitudes that cannot damage the actuator. If an individual is mathematically invalid or poses a risk to the actuator, it is promptly removed. Table I summarizes the parameters and probabilities used in our implementation of GP control.

IV. RESULTS AND DISCUSSION

A. Uncontrolled system: Baseline characteristics

Before presenting the results from GP control, it is helpful to examine the baseline characteristics of the uncontrolled system, whose operating conditions were reported in Sec. II. This system is

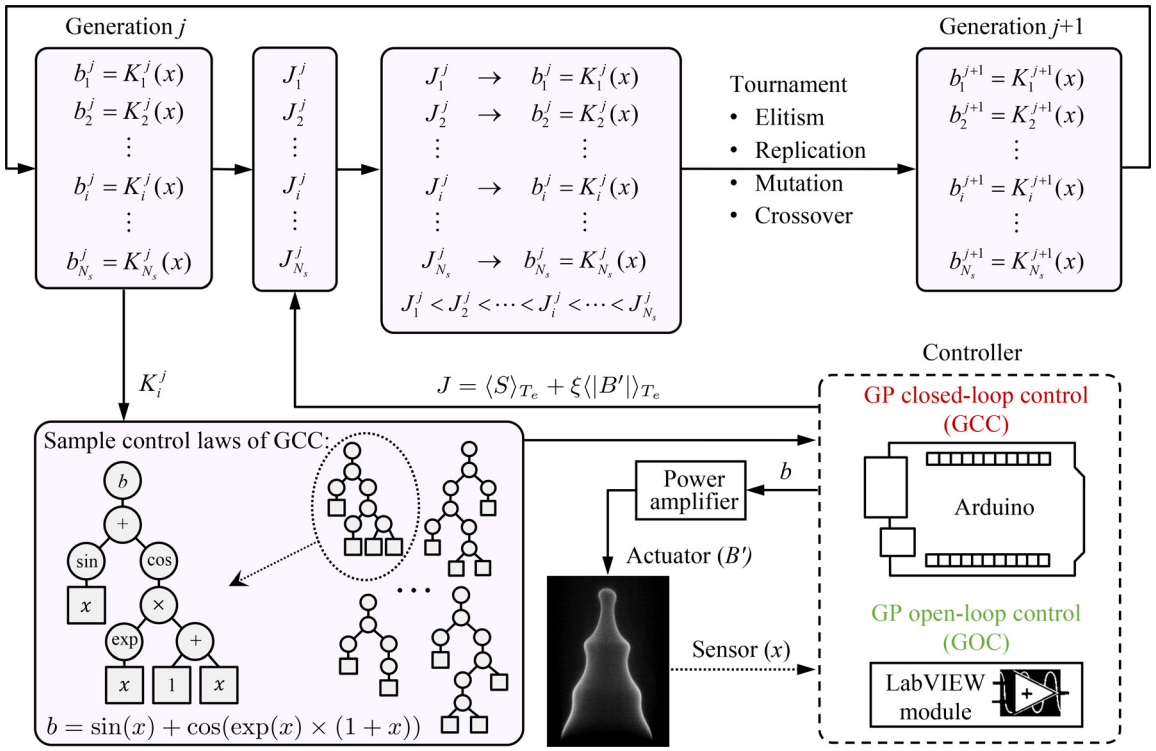

FIG. 2. Architecture of the GP control framework with two main loops:[22] a slow loop for discovering individuals via GP, and a fast loop for real-time feedback control. Here, K_i^j is the ith individual of the jth generation, and J_i^j is its cost function.

TABLE I. Parameters and probabilities of the GP algorithm.

Parameters or probabilities	Value
Number of generations, N_g	10
Size of a generation, N_s	Generation 1: 100 Generations 2–10: 60
Number of elite individuals, N_E	5 (+1 with each gen.)
Crossover probability, P_c	0.5
Mutation probability, P_m	0.4
Replication probability, P_r	0.1
Evaluation time, T_e	2 s
Penalization coefficient, ξ	1.5
Constant range	$[-3, 3]$
Node functions	$+, -, \times, /$, sin, cos, exp, log

thermoacoustically unstable, with self-excited limit-cycle oscillations occurring at a natural frequency of $f_n = 255 \pm 1.5$ Hz.[16] From this f_n value and a mean fluid temperature of $185 \pm 5\,^{\circ}$C in the combustor, the half-wavelength of an acoustic standing mode is 866 mm, which is close to the combustor length ($L = 860$ mm). As the combustor is open at both ends, this indicates a fundamental standing mode, with pressure nodes at both ends and a pressure anti-node near the middle.[16] This explains why the microphone is located near the middle of the combustor (see Sec. II: $z/L = 0.45$).

B. GP closed-loop control (GCC)

First, we show in Fig. 3 the convergence history of GCC in terms of J. As the number of generations increases from $j = 1$ to 10, more and more individuals can achieve J values approaching 0 [Fig. 3(a)]. Here, the J values of the best 30 individuals of each generation are shown, with the last generation ($j = 10$) highlighted in red. The rapid convergence of the GP algorithm can also be seen in Fig. 3(b), which shows the average J of the best 10 individuals of each generation, $\bar{J}^j_{1-10}$. As the number of generations increases, $\bar{J}^j_{1-10}$ starts off near 1 but rapidly approaches 0 after just the second generation. Thus, for conservativeness, we breed a total of $N_g = 10$ generations before extracting the optimal GCC individual, defined here to be the GCC individual with the lowest value of J.

Next, we visualize the control landscape on a 2D proximity map. We use classic multi-dimensional scaling[39] to find a centered representation of points $\Gamma = [\gamma_1, \gamma_2, \ldots, \gamma_N]$ with $\gamma_1, \gamma_2, \ldots, \gamma_N \in \mathbb{R}^2$ such that the pairwise distances of the individuals approximate the true distances. To quantify the dissimilarity between any two individuals, K_m and K_n with $1 \le m, n \le N$, we define the matrix $D_{m,n} = [(B'_{rms,m} - B'_{rms,n})^2 + (\eta_m - \eta_n)^2]^{1/2} + \alpha |J_m - J_n|$. Here, $\eta \equiv (p'_{rms} - p'_{rms,*})/p'_{rms,*}$, where p'_{rms} and $p'_{rms,*}$ denote the root mean square (rms) of the pressure fluctuations with and without control, respectively. The first term is the difference between two individuals in terms of the actuator power and the thermoacoustic amplitude reduction, while the second term penalizes the difference between their J values, with $\alpha = 1$ used to smoothen the control landscape.[22]

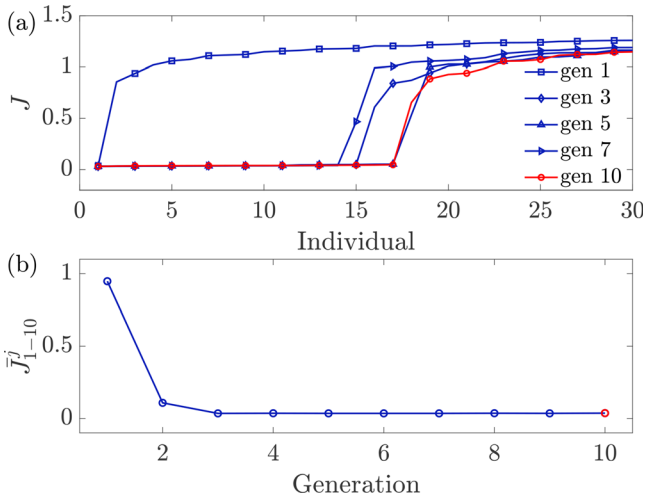

FIG. 3. Convergence history of GCC: (a) J values for the best 30 individuals of each generation and (b) the average J of the best ten individuals of each generation, both shown as the number of generations increases from $j = 1$ to 10.

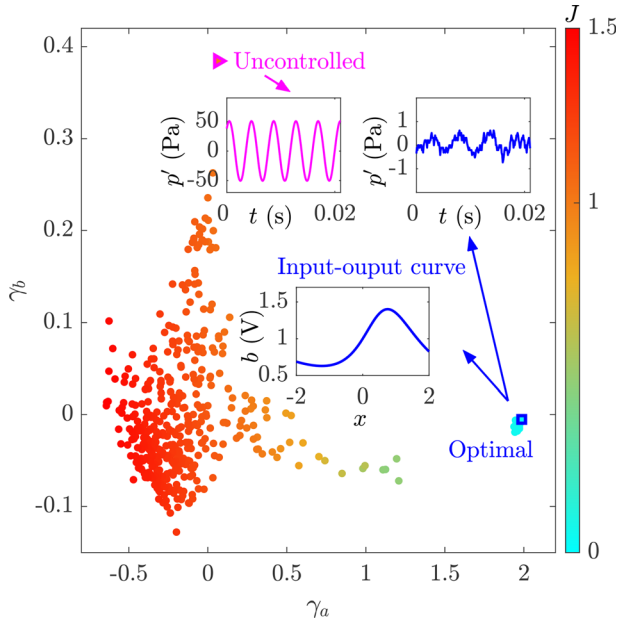

FIG. 4. Control landscape on a 2D proximity map containing all the GCC individuals, including the optimal one (blue square) and the uncontrolled case (magenta triangle). Representative time traces of p' are also shown, alongside the input–output curve for the optimal GCC individual.

Figure 4 shows the control landscape on a 2D proximity map defined by $[\gamma_a, \gamma_b] \in \mathbb{R}^2$. Each GCC individual is represented by a discrete marker whose color corresponds to its J value, with the uncontrolled case (magenta triangle) shown as the baseline. A total of 640 individuals are tested, but only 446 unique individuals are shown in Fig. 4 because some are duplicates or lead to flame blow-off. This proximity map reveals that the best GCC individuals (i.e., those with low J) cluster near a spot on the far right, with the rest forming a distributed arc along the bottom left. The optimal GCC individual has an exceedingly low value of the cost function ($J = 0.030$), with a functional form of $b(x) = \exp(x/(\exp(x) - x) + \sin(\sin(-3.0)) \times 2x)$. The functional forms of the top 25 GCC individuals, and their input–output curves, can be found in the Appendix.

Figure 5 shows time traces of p' and B' for the optimal GCC individual from Fig. 4. After GCC is activated at $t = 1$ s, the amplitude of p' drops rapidly from an uncontrolled value of 50 Pa [Fig. 5(b)] to a controlled value of around 1 Pa [Fig. 5(d)]. After this initial transient, p' remains at a negligible level, while B' remains within ± 40 mV following a starting burst. This low-amplitude state persists until GCC is deactivated at $t = 9$ s, after which the system returns to its original (uncontrolled) state without any signs of hysteresis. Figure 5(b) shows that B' fluctuates significantly at large positive values but appears truncated at large negative values. The former and latter features can be attributed to the hump part ($x \approx +1$) and flat part ($x \approx -1$), respectively, of the optimal input–output curve shown in Fig. 4 (inset). Moreover, a strong degree of correlation can be seen between the p' and B' signals at low $|p'|$ [Figs. 5(c) and 5(d)]. This occurs because the input–output curve of the optimal GCC individual is approximately linear when $x \approx 0$ [see Fig. 4 (inset)], which enables phase information to pass directly from p' to B', enhancing their correlation.

To understand the actuation mechanism learned by GCC, we examine the power spectral density (PSD) of B' for 20 elite individuals [Fig. 6(a)] and 30 non-elite individuals [Fig. 6(b)]. Almost all the elite individuals, including the optimal GCC individual, share a common PSD signature [Fig. 6(a)]: the highest peak is at the natural frequency of the self-excited thermoacoustic mode (f_n) and is accompanied by weaker harmonics ($2f_n$ and $3f_n$), while a strong peak appears at a seemingly arbitrary frequency of $f_g = 0.77 f_n$. Later, we will see that f_g actually corresponds to the frequency of maximum gain for the open (unconfined) flame. By contrast, none of the non-elite individuals shows any evidence of the f_g mode in the PSD [Fig. 6(b)]. Thus, we conclude that excitation at f_g plays a pivotal role in suppressing the self-excited thermoacoustic oscillations of this combustion system.

To explore the evolution of the f_g mode, we show in Fig. 7 the PSD of B', p', and q' over time. Before GCC is activated at $t = 1$ s, both p' and q' oscillate predominantly at f_n. After GCC is activated, the dominant frequency of p' and q' remains at f_n initially but then switches to f_g, although its amplitude is relatively low. This coincides exactly with a switch in spectral energy from f_n to f_g in B' [Fig. 7(a)] along with a marked drop in the amplitude of p' (Fig. 5), providing evidence of a link between the f_g mode and the thermoacoustic amplitude.

To identify the physical origin of the f_g mode, we note that Roy *et al.*[40] recently investigated the open-loop control of self-excited thermoacoustic oscillations in a laminar premixed combustor. They showed that the inherent flame dynamics play a key role in determining the actuation frequency at which oscillation quenching occurs. Thus, we perform additional experiments without the combustor installed, leaving the flame unconfined and hence free of acoustic resonance. We subject the open flame to open-loop time-periodic acoustic forcing at different frequencies (f_f) and amplitudes ($u'/\bar{u}$); here, u' is the amplitude of the velocity perturbations at the burner exit and $\bar{u}$ is the time-averaged bulk velocity of the premixed reactants.[16] Figure 8 shows the

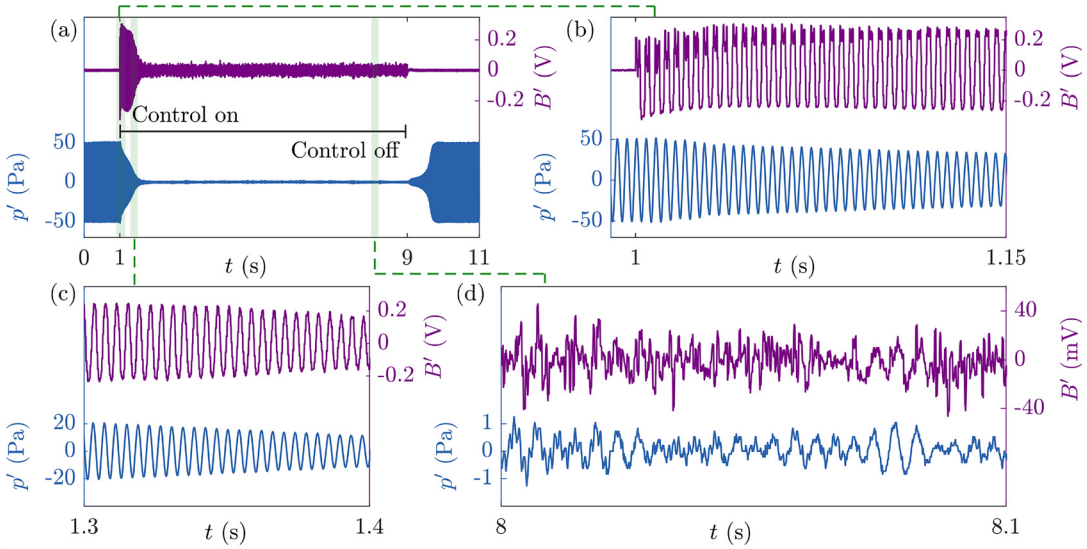

FIG. 5. Optimal GCC individual from Fig. 4: time traces of p' and B' for different temporal window sizes.

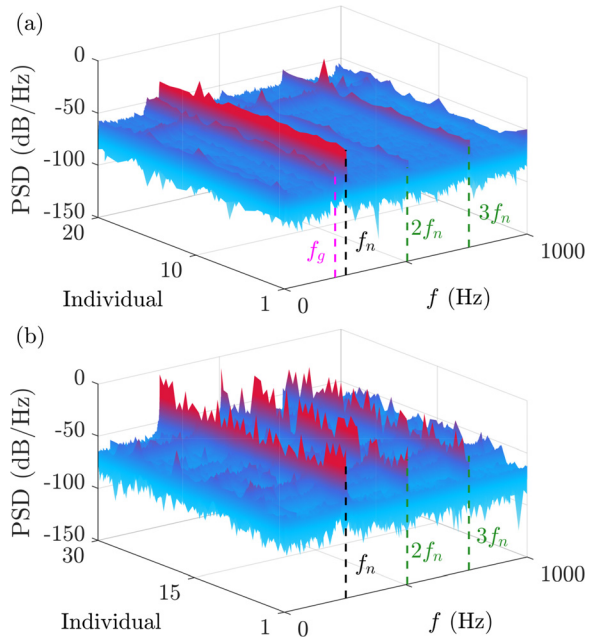

FIG. 6. Various GCC individuals: PSD of B' from (a) 20 elite individuals, with the optimal GCC individual from Fig. 4 shown as "Individual 1," and (b) 30 poorly performing individuals selected from the non-elite group.

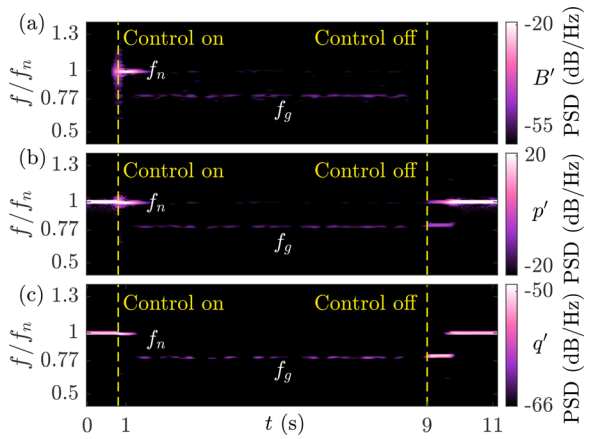

FIG. 7. Optimal GCC individual from Fig. 4: PSD of (a) B', (b) p', and (c) q' as a function of time. GCC is activated at $t = 1$ s and deactivated at $t = 9$ s.

gain $G = |(q'/\bar{q})/(u'/\bar{u})|$ of the flame describing function.[10,41] A pronounced peak in G appears at $f_g = 0.77 f_n$ for low $u'/\bar{u}$, indicating that the HRR response of the open flame is exceptionally strong at this specific frequency. We speculate that this is why GCC has decided to act at f_g: it has learned to exploit the strong amplification at that frequency, efficiently converting even low-power actuation into a large reduction in thermoacoustic amplitude, possibly via asynchronous quenching.[15,16,40] It is promising how GCC can identify this actuation mechanism involving the preferred mode (f_g) of the open flame, even though it has only ever seen the flame in an acoustically coupled configuration.

C. Benchmarking GCC against GOC and OLC

We now benchmark the optimal individual from GCC (Sec. IV B) against those from GOC and OLC. For GOC, we use linear GP control[22,30] to optimize the parameters of harmonic functions within an open-loop framework. We implement this experimentally using a LabVIEW module, rather than the micro-controller from Sec. IV B (Fig. 1). The GOC individuals are formulated as $b(t) = K[x(t)]$, where $x(t)$ is a harmonic function encapsulating the input. We define $x_i(t) = \sin(2\pi k_i f_n t)$, where k_i ranges from 0.2 to 3 with a step

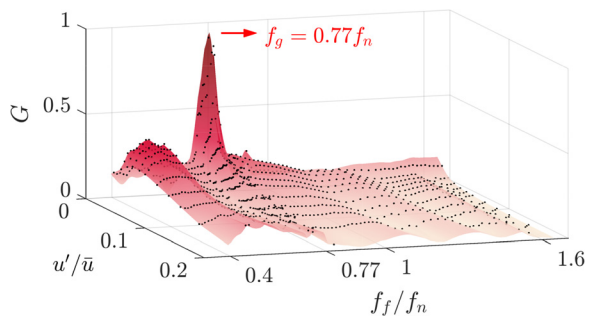

FIG. 8. Gain of the flame describing function with no combustor installed. The frequency at maximum gain for low $u'/\bar{u}$ is $f_g = 0.77 f_n$, which matches the dominant frequency of B' seen in the optimal GCC individual from Fig. 4.

size of 0.01. After ten generations, the optimal GOC individual is found to be $b(t) = 0.7\sin[\cos(x(t))]$ with $x(t) = \sin(2\pi k f_n t)$ and $k = 0.41$. For OLC, we refer to the results of our previous study.[16]

Figure 9 uses Pareto diagrams to compare the three control strategies (GCC, GOC, OLC) in a parameter space defined by the input cost (B'_{rms}) and the state cost (η). For GCC [Fig. 9(a)], the best individuals are located at the bottom left, producing a large reduction in thermoacoustic amplitude with minimal actuation power. The worst individuals are distributed toward the top right, where some can actually increase the thermoacoustic amplitude relative to the uncontrolled state ($\eta > 0$). For GOC [Fig. 9(b)], a similar pattern to GCC is observed, except that the worst individuals are lined up at $\eta \approx 0$, implying that they have little influence on the thermoacoustic amplitude, irrespective of the actuation power consumed. For OLC [Fig. 9(c)], the best control laws are again located at the bottom left, but the rest are more broadly distributed than those from GCC and GOC owing to the brute force nature of the open-loop mapping strategy.[16] Figure 9(d) shows a magnified view of the best individuals from all three control strategies. The optimal individuals (K_{GCC}, K_{GOC}, K_{OLC}), as defined by the lowest J, are highlighted with hollow magenta markers. We find that K_{GCC} outperforms both K_{GOC} and K_{OLC} in two ways: it produces the largest reduction in thermoacoustic amplitude (η) while consuming the least actuator power (B'_{rms}), thereby yielding the lowest J value among all three control strategies. The superiority of GCC can be seen quantitatively in Fig. 10, which compares not just the optimal individuals with the lowest J (K_{GCC}, K_{GOC}, K_{OLC}) but also the GOC and OLC individuals with the lowest η ($K_{GOC,\eta}$, $K_{OLC,\eta}$). We find that K_{GOC}, $K_{GOC,\eta}$, K_{OLC}, and $K_{OLC,\eta}$ can all achieve similar levels of thermoacoustic amplitude reduction as K_{GCC} (namely, $\eta \approx -96$ to -99%), but the former individuals require 2.7 to 9.2 times the voltage as K_{GCC}. This explains why K_{GCC} has such a low value of the cost function ($J = 0.030$) in comparison with the other control strategies.

V. CONCLUSIONS

In this experimental study, we have demonstrated that self-excited thermoacoustic oscillations in a laminar premixed combustor can be suppressed efficiently using genetic programing (GP). This is a data-driven machine learning framework that enables control laws (i.e., individuals) to be discovered even without access to a system model. It relies on an evolutionary algorithm to make decisions based on natural selection: individuals in a generation compete at a control

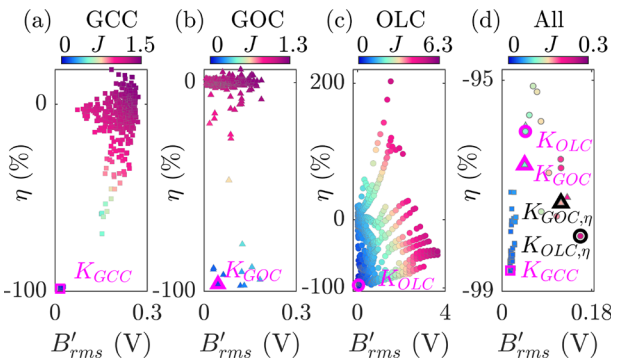

FIG. 9. Pareto diagrams for (a) GCC, (b) GOC, (c) OLC, and (d) all three control strategies. The optimal individuals (K_{GCC}, K_{GOC}, K_{OLC}), as defined by the lowest J, are highlighted with hollow magenta makers. In panel (d), the GOC and OLC individuals with the lowest η (not the lowest J) are highlighted with hollow black markers. The GCC individual with the lowest η is also the optimal GCC individual K_{GCC}.

task defined by a cost function. The performance of each individual is evaluated, and rules are set to spread the genes of successful individuals to the next generation. In this way, optimal solutions can be identified in a diverse search space.

First, we applied GP closed-loop control (GCC) to the combustor using a single sensor (pressure transducer) and a single actuator (loudspeaker). We found that the optimal GCC individual can reduce the thermoacoustic amplitude by over 98% relative to the uncontrolled state while consuming only minimal actuator power. In benchmarking tests, we found that GCC can outperform both GP open-loop control (GOC) and conventional open-loop control (OLC) based on time-periodic forcing, achieving not just the largest reduction in thermoacoustic amplitude but also consuming the least actuator power.

The efficiency of GCC was attributed to the GP algorithm learning by itself an actuation mechanism that exploits the strong amplification of the heat-release-rate (HRR) response of the open flame at its preferred mode. This mode corresponds to the frequency at which the

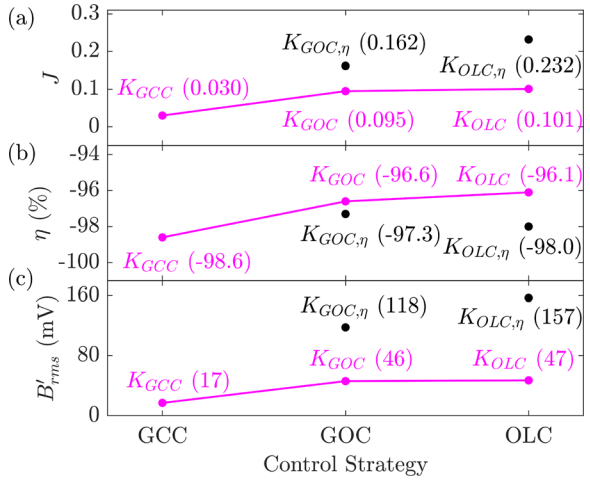

FIG. 10. Comparison of the (a) cost function, (b) thermoacoustic amplitude reduction, and (c) actuator voltage for the five individuals highlighted in Fig. 9(d).

gain of the flame describing function peaks at low perturbation amplitudes. The GP algorithm could identify and exploit this strong HRR amplification of the open flame for thermoacoustic suppression, despite only ever seeing the flame in its acoustically coupled configuration (i.e., surrounded by a combustor). Current work includes applying GCC to turbulent combustors with additional degrees of freedom where the dynamics are dominated by strong nonlinearity, multi-scale flow structures, and noisy high-dimensional features.

ACKNOWLEDGMENTS

This work was supported by the Research Grants Council of Hong Kong (Project No. 16210419).

AUTHOR DECLARATIONS

Conflict of Interest

The authors have no conflicts to disclose.

Author Contributions

Bo Yin: Data curation (lead); Formal analysis (equal); Investigation (equal); Methodology (equal); Software (equal); Visualization (equal); Writing – original draft (equal); Writing – review & editing (equal). **Zhijian Yang:** Investigation (equal). **Yu Guan:** Investigation (equal); Methodology (equal). **Stephane Redonnet:** Formal analysis (equal); Investigation (equal); Writing – review & editing (equal). **Vikrant Gupta:** Formal analysis (equal); Investigation (equal); Writing – review & editing (equal). **Larry K. B. Li:** Conceptualization (lead); Formal analysis (lead); Funding acquisition (lead); Investigation (lead); Methodology (lead); Project administration (lead); Supervision (lead); Visualization (lead); Writing – original draft (lead); Writing – review & editing (lead).

DATA AVAILABILITY

The data that support the findings of this study are available from the corresponding author upon reasonable request.

APPENDIX: TOP-PERFORMING GP FEEDBACK CONTROL LAWS

In Table II, we show the functional forms of the top 25 GCC individuals from the entire GP evaluation process across all ten generations. These individuals ($K_1 - K_{25}$) are sorted by the value of the cost function J. Their corresponding input–output curves are shown in Fig. 11. We find that nearly all the input–output curves exhibit an S-shaped trend. From Table II, we find that most of the individuals contain similar branches because these top-performing

TABLE II. The top 25 GCC individuals sorted by the cost function J.

Individual	Functional form	J
K_1	$b = \exp(x/(\exp(x) - x)) \times \exp(\sin(\sin(-3.0)) \times 2x)$	0.0302
K_2	$b = \exp(x/(\exp(x) - \sin(x))) \times \exp(\sin(\sin(-3.0)) \times (x + \sin(x)))$	0.0307
K_3	$b = \exp(x/(\exp(x) - x)) \times \exp(\sin(\sin(-3.0)) \times (x + \sin(x)))$	0.0317
K_4	$b = \exp(x/(\exp(x) - \sin(x))) \times \exp(\sin(\sin(-3.0)) \times 2x)$	0.0318
K_5	$b = \exp(x/(\exp(x) - x)) \times \exp(\sin(-3.0) \times 2\sin(x))$	0.0319
K_6	$b = \exp(x/(\exp(x) - x)) \times \exp(\sin(-3.0) \times (x + \sin(x)))$	0.0321
K_7	$b = \exp(x/(\exp(x) - \sin(x))) \times \exp(\sin(-3.0) \times 2x)$	0.0327
K_8	$b = \exp(x/(\exp(x) - \sin(x))) \times \exp(\sin(-3.0) \times (x + \sin(x)))$	0.0334
K_9	$b = \exp(x/(\exp(x) - \sin(x))) \times \exp(\sin(-3.0) \times 2\sin(x))$	0.0336
K_{10}	$b = \exp(x/(\exp(x) - x)) \times \exp(\sin(-3.0) \times 2x)$	0.0348
K_{11}	$b = \exp(x/(\exp(x) - x)) \times \exp(\sin(-3.0) \times x)$	0.0358
K_{12}	$b = \exp(x/(\exp(x) - x)) \times \exp(\sin(-3.0) \times (2x - 0.3))$	0.0362
K_{13}	$b = \exp(x) \times \exp(\log(\cos(x)) \times 2x)$	0.0367
K_{14}	$b = \exp(x/(\exp(x) - x)) \times \exp(\sin(-3.0) \times (\sin(-3.0) + \sin(x)))$	0.0368
K_{15}	$b = \exp(x/(\exp(x) - x)) \times \exp(\sin(\sin(-3.0)) \times x)$	0.0368
K_{16}	$b = \exp(x/(\exp(x) - x)) \times \exp(\sin(-3.0) \times (\sin(-3.0) + x))$	0.0372
K_{17}	$b = \exp(\cos(1.4 \times \sin(-2.5)) \times \sin(\sin(\sin(x))))$	0.0386
K_{18}	$b = \exp(x/(\exp(x) - x)) \times \exp(\sin(\sin(-3.0)) \times (\sin(x) + \sin(x)))$	0.0422
K_{19}	$b = \exp(x/(\exp(x) - \sin(x))) \times \exp(\sin(-3.0) \times (\sin(x) + 0.9))$	0.0449
K_{20}	$b = \exp(x/(\exp(x) - \sin(x))) \times \exp(\sin(-3.0) \times (-0.9 + x))$	0.0453
K_{21}	$b = \exp(0.7 \times \sin(\sin(x)))$	0.0469
K_{22}	$b = \exp(\exp(\sin(-2.5 + x \times \cos(2.3)))) - \cos(\cos((\sin(-0.9) + x) \times \cos(x))))$	0.0481
K_{23}	$b = \exp(x/(\exp(x) - \sin(x))) \times \exp(\sin(\sin(-3.0)) \times (-0.8 + x))$	0.0515
K_{24}	$b = \exp(x) \times \exp(\log(\cos(x)) \times x)$	0.0546
K_{25}	$b = \exp((\sin(-x) - \sin(x))/(-\exp(x) + x - 1.5))$	0.0563

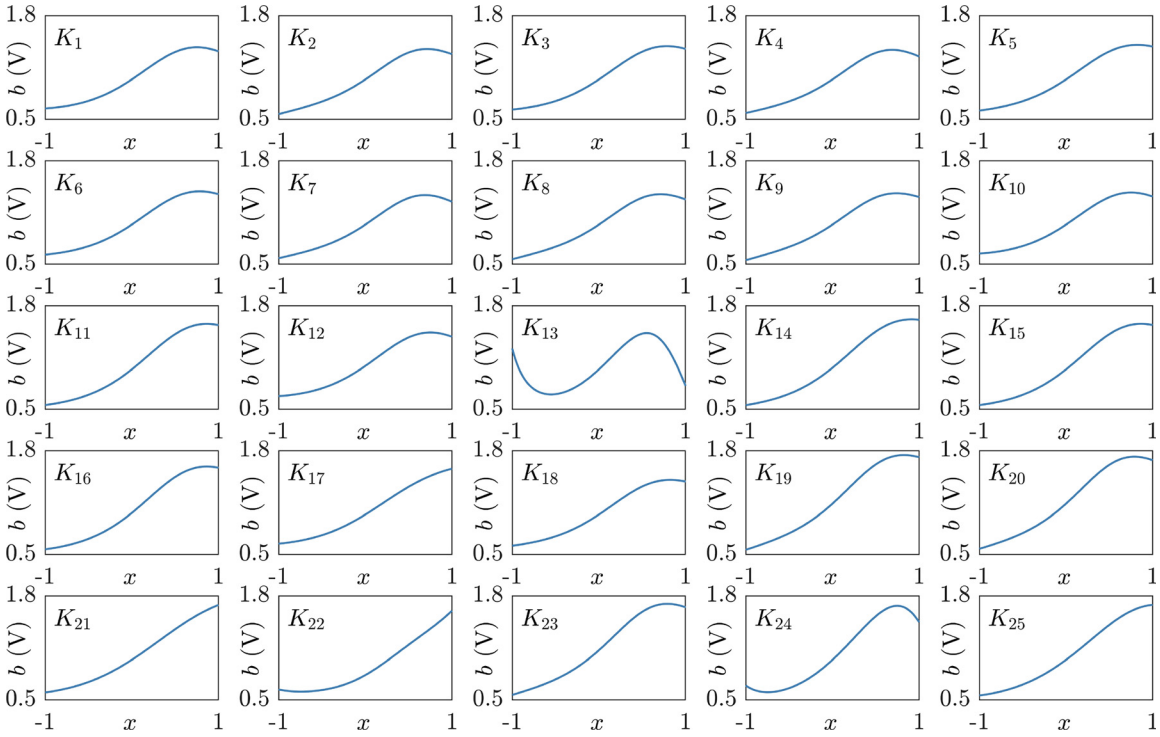

FIG. 11. Input–output curves of the top 25 GCC individuals listed in Table II. Here, x and b are the input and output of the individuals, respectively.

individuals have either inherited directly the genes from previous generations or have been created by genetic operations involving elite individuals from previous generations. In our experiments, the GP input is always within the range $-\pi/2 < x < \pi/2$, which is why $\log[\cos(x)]$—but not $\log[\sin(x)]$—appears in the functional forms.

REFERENCES

[1]T. Poinsot, "Prediction and control of combustion instabilities in real engines," Proc. Combust. Inst. **36**, 1–28 (2017).

[2]S. Shima, K. Nakamura, H. Gotoda, Y. Ohmichi, and S. Matsuyama, "Formation mechanism of high-frequency combustion oscillations in a model rocket engine combustor," Phys. Fluids **33**, 064108 (2021).

[3]T. C. Lieuwen and V. Yang, *Combustion Instabilities in Gas Turbine Engines: Operational Experience, Fundamental Mechanisms, and Modeling* (American Institute of Aeronautics and Astronautics, 2005).

[4]S. Candel, "Combustion dynamics and control: Progress and challenges," Proc. Combust. Inst. **29**, 1–28 (2002).

[5]Y. Huang and V. Yang, "Dynamics and stability of lean-premixed swirl-stabilized combustion," Prog. Energy Combust. **35**, 293–364 (2009).

[6]S. Murayama and H. Gotoda, "Attenuation behavior of thermoacoustic combustion instability analyzed by a complex-network-and synchronization-based approach," Phys. Rev. E **99**, 052222 (2019).

[7]X. Zhao, D. Zhao, C. M. Shelton, B. Wang, X. Dong, J. Li, and Y. Huang, "Outlet boundary condition and mean temperature gradient effects on the minimum acoustics disturbances energy in triggering nonlinear thermoacoustic instability," Phys. Fluids **36**, 034117 (2024).

[8]H. Gotoda, Y. Shinoda, M. Kobayashi, Y. Okuno, and S. Tachibana, "Detection and control of combustion instability based on the concept of dynamical system theory," Phys. Rev. E **89**, 022910 (2014).

[9]M. P. Juniper and R. I. Sujith, "Sensitivity and nonlinearity of thermoacoustic oscillations," Annu. Rev. Fluid Mech. **50**, 661–689 (2018).

[10]T. Schuller, T. Poinsot, and S. Candel, "Dynamics and control of premixed combustion systems based on flame transfer and describing functions," J. Fluid Mech. **894**, P1 (2020).

[11]W. Polifke, "Modeling and analysis of premixed flame dynamics by means of distributed time delays," Prog. Energy Combust. Sci. **79**, 100845 (2020).

[12]G. Xu, B. Wang, B. Jin, Z. Wang, and P. Liu, "Numerical study of triggered thermoacoustic instability driven by linear and nonlinear combustion response in a solid rocket motor," Phys. Fluids **36**, 034110 (2024).

[13]K. R. McManus, U. Vandsburger, and C. T. Bowman, "Combustor performance enhancement through direct shear layer excitation," Combust. Flame **82**, 75–92 (1990).

[14]B. D. Bellows, A. Hreiz, and T. C. Lieuwen, "Nonlinear interactions between forced and self-excited acoustic oscillations in premixed combustor," J. Propul. Power **24**, 628–631 (2008).

[15]S. Mondal, S. A. Pawar, and R. I. Sujith, "Forced synchronization and asynchronous quenching of periodic oscillations in a thermoacoustic system," J. Fluid Mech. **864**, 73–96 (2019).

[16]Y. Guan, V. Gupta, K. Kashinath, and L. K. B. Li, "Open-loop control of periodic thermoacoustic oscillations: Experiments and low-order modelling in a synchronization framework," Proc. Combust. Inst. **37**, 5315–5323 (2019).

[17]D. Zhao, Z. Lu, H. Zhao, X. Li, B. Wang, and P. Liu, "A review of active control approaches in stabilizing combustion systems in aerospace industry," Prog. Aerosp. Sci. **97**, 35–60 (2018).

[18]R. I. Sujith and V. R. Unni, "Complex system approach to investigate and mitigate thermoacoustic instability in turbulent combustors," Phys. Fluids **32**, 061401 (2020).

[19]J. P. Hathout, A. M. Annaswamy, M. Fleifil, and A. F. Ghoniem, "A model-based active control design for thermoacoustic instability," Combust. Sci. Technol. **132**, 99–138 (1998).

[20]D. U. Campos-Delgado, K. Zhou, D. Allgood, and S. Acharya, "Active control of combustion instabilities using model-based controllers," Combust. Sci. Technol. **175**, 27–53 (2003).

[21]A. P. Dowling and A. S. Morgans, "Feedback control of combustion oscillations," Annu. Rev. Fluid Mech. **37**, 151–182 (2005).

[22]T. Duriez, S. L. Brunton, and B. R. Noack, *Machine Learning Control-Taming Nonlinear Dynamics and Turbulence* (Springer, 2017), Vol. 116.
[23]J. Koza, "Genetic programming as a means for programming computers by natural selection," Stat. Comput. **4**, 87–112 (1994).
[24]N. Gautier, J. L. Aider, T. Duriez, B. Noack, M. Segond, and M. Abel, "Closed-loop separation control using machine learning," J. Fluid Mech. **770**, 442–457 (2015).
[25]A. Debien, K. A. F. F. Krbek, N. Mazellier, T. Duriez, L. Cordier, B. R. Noack, M. W. Abel, and A. Kourta, "Closed-loop separation control over a sharp edge ramp using genetic programming," Exp. Fluids **57**, 40 (2016).
[26]V. Parezanović, L. Cordier, A. Spohn, T. Duriez, B. R. Noack, J. P. Bonnet, M. Segond, M. Abel, and S. L. Brunton, "Frequency selection by feedback control in a turbulent shear flow," J. Fluid Mech. **797**, 247–283 (2016).
[27]R. Li, B. R. Noack, L. Cordier, J. Borée, and R. Harambat, "Drag reduction of a car model by linear genetic programming control," Exp. Fluids **58**, 103 (2017).
[28]C. Raibaudo, P. Zhong, B. R. Noack, and R. J. Martinuzzi, "Machine learning strategies applied to the control of a fluidic pinball," Phys. Fluids **32**, 015108 (2020).
[29]Y. Zhou, D. Fan, B. Zhang, R. Li, and B. R. Noack, "Artificial intelligence control of a turbulent jet," J. Fluid Mech. **897**, A27 (2020).
[30]Y. Liu, J. Tan, H. Li, Y. Hou, D. Zhang, and B. R. Noack, "Simultaneous control of combustion instabilities and NO_x emissions in a lean premixed flame using linear genetic programming," Combust. Flame **251**, 112716 (2023).
[31]M. Murugesan and R. I. Sujith, "Combustion noise is scale-free: Transition from scale-free to order at the onset of thermoacoustic instability," J. Fluid Mech. **772**, 225–245 (2015).
[32]M. Lee, Y. Guan, V. Gupta, and L. K. B. Li, "Input-output system identification of a thermoacoustic oscillator near a Hopf bifurcation using only fixed-point data," Phys. Rev. E **101**, 013102 (2020).
[33]M. Lee, K. T. Kim, V. Gupta, and L. K. B. Li, "System identification and early warning detection of thermoacoustic oscillations in a turbulent combustor using its noise-induced dynamics," Proc. Combust. Inst. **38**, 6025–6033 (2021).
[34]Y. Guan, W. He, M. Murugesan, Q. Li, P. Liu, and L. K. B. Li, "Control of self-excited thermoacoustic oscillations using transient forcing, hysteresis and mode switching," Combust. Flame **202**, 262–275 (2019).
[35]Y. Guan, V. Gupta, M. Wan, and L. K. B. Li, "Forced synchronization of quasiperiodic oscillations in a thermoacoustic system," J. Fluid Mech. **879**, 390–421 (2019).
[36]Y. Guan, B. Yin, Z. Yang, and L. K. B. Li, "Forced synchronization of self-excited chaotic thermoacoustic oscillations," J. Fluid Mech. **982**, A9 (2024).
[37]E. T. Signor, C. M. Shelton, and J. Majdalani, "Characterization of the acoustic pressure waveforms in Rijke tubes with spatially varying heat sources and temperature distributions," Phys. Fluids **36**, 034113 (2024).
[38]J. Chen, H. Zong, H. Song, Y. Wu, H. Liang, and Z. Su, "Closed-loop plasma flow control of a turbulent cylinder wake flow using machine learning at Reynolds number of 28 000," Phys. Fluids **36**, 015123 (2024).
[39]G. Young and A. S. Householder, "Discussion of a set of points in terms of their mutual distances," Psychometrika **3**, 19–22 (1938).
[40]A. Roy, S. Mondal, S. A. Pawar, and R. I. Sujith, "On the mechanism of open-loop control of thermoacoustic instability in a laminar premixed combustor," J. Fluid Mech. **884**, A2 (2020).
[41]N. Noiray, D. Durox, T. Schuller, and S. Candel, "A unified framework for nonlinear combustion instability analysis based on the flame describing function," J. Fluid Mech. **615**, 139–167 (2008).